# Detection of the formyl radical by EPR spin-trapping and mass spectrometry

Norbert A. Bauer[a,*], Enamul Hoque[a], Manfred Wolf[a], Karin Kleigrewe[b] and Thomas Hofmann[b]

[a]Helmholtz Zentrum München - German Research Center for Environmental Health, Institute of Groundwater Ecology, Ingolstädter Landstrasse 1, 85764 Neuherberg, Germany.

[b]Bavarian Center for Biomolecular Mass Spectrometry (BayBioMS), Technical University of Munich, Gregor-Mendel-Strasse 4, 85354 Freising, Germany.

*Corresponding author
Norbert A. Bauer
Helmholtz Zentrum München – German Research Center for Environmental Health,
Institute of Groundwater Ecology, Ingolstädter Landstr.1, 85764 Neuherberg, Germany,
Phone: +49-89-31872579, Fax +49-89-31873361

E-mail addresses:
bauer@wzw.tum.de (Norbert A. Bauer)
hoque@helmholtz-muenchen.de (Enamul Hoque)
manfred.f.wolf@gmail.com (Manfred Wolf)
karin.kleigrewe@tum.de (Karin Kleigrewe)
thomas.hofmann@tum.de (Thomas Hofmann)

Running title: Detection of formyl radical

Keywords: Formyl radical, EPR, Simulation, Mass spectrometry, DMPO, Ambient temperature

Funding information: This research was funded by Federal Government of Germany and Bavarian State Government. This work was supported by the Helmholtz Forschungszentrum München, (Grant/Award Number: ´G-504300-002´).

## A B S T R A C T

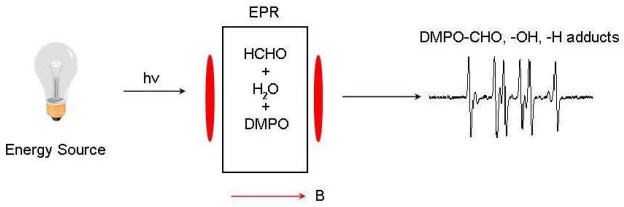


For the first time we here present the unambiguous identification of the formyl radical ($^{\bullet}$CHO) by EPR (Electron Paramagnetic Resonance) spectroscopy and mass spectrometry (MS) using DMPO (5,5-dimethyl-1-pyrroline N-oxide) as spin trap at ambient temperature without using any catalysator(s). The $^{\bullet}$CHO was continuously generated by UV photolysis in closed anoxic environment from pure formaldehyde (HCHO) in aqueous solution. The isotropic hyperfine structure constants of $^{\bullet}$CHO were determined as $a_N$ = 15.72 G and $a_H$ = 21.27 G. The signals were deconvoluted and split by simulation in their single adduct components: DMPO-CHO, DMPO-H and DMPO-OH. We verified our results at first using MNP (2-methyl-2-nitroso-propane) as spin trap with known literature data and then mass spectrometry. Similarly the MNP adduct components MNP-CHO, MNP-H as well as its own adduct, the MNP-2-methyl-2-propyl (MNP-MP) were deconvoluted. Due to the low signal intensities, we had to accumulate single measurements for both spin traps. Using MS we got the exact mass of the reduced $^{\bullet}$CHO adduct independently confirming the result of EPR detection of formyl radical.

## 1. Introduction

The formyl radical ($^{\bullet}$CHO) is an oxygen containing molecule formed e. g. in course of oxidation of hydrocarbons. It is of considerable importance as an intermediate in chemical [1-3] as well as in biochemical reactions [4, 5]. Measurements of $^{\bullet}$CHO at 77 K in single crystals were carried out by Holmberg [6] and adsorption to transition metal surfaces by Gomes and Gomes [7]. The EPR spectra of the $^{\bullet}$CHO and the deuterated $^{\bullet}$CDO were observed in solid carbon monoxide between temperatures of 4.2 to 30 K [8]. This radical was also detected in interstellar molecular clouds [9]. The technique used was the measurement of the strongest hyperfine component of one of its microwave transitions. Measurements of $^{\bullet}$CHO at very low or high temperatures or under metal catalyzed conditions are of no relevance for biological and medical processes. It is now believed that in connection with cancer the human body produces formaldehyde (HCHO). This is probably caused by the aggressive formyl radical [10]. Yang et al. [11] assume to have detected the $^{\bullet}$CHO in their process experiments and used an aqueous dispersion of catalytic Pt/$TiO_2$ powders containing DMPO and HCHO. Indeed we can confirm their assumption, as we found similar hyperfine structure constants.

Spin trapping of short-living radical intermediates $^{\bullet}$R by nitrones and other spin traps is also a well-known technique [12, 13]. The resultant DMPO spin adduct is a relatively stable nitrone radical, which can be characterized by EPR. The basic reaction for the appearing radical adduct with DMPO is shown in Scheme 1.

**Scheme 1.** DMPO reaction with a radical. The structure and radical electron are indicated ($^{\bullet}$R = $^{\bullet}$CHO, $^{\bullet}$H, $^{\bullet}$OH or other components for different investigations).

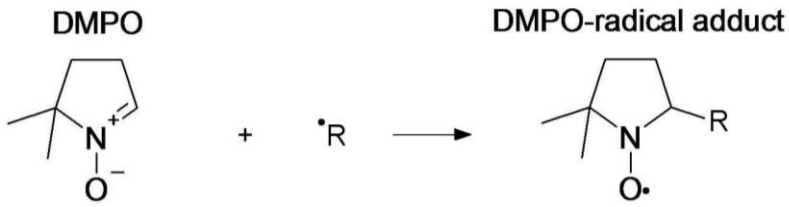


The formyl radical is involved in a series of many abiotic and biotic reactions. It is the starting point of many biosynthetic reaction sequences of important metabolic products involved in the evolution of life [14]. The propulsive chemical force for these reactions is assumed to be the hydrogen radical.

In the present study we will provide evidence for the detection of $^{\bullet}$CHO and $^{\bullet}$H in combination with $^{\bullet}$OH upon UV photolysis of HCHO at ambient temperature applying DMPO. DMPO causes less lipid peroxidation [15] and is EPR silent. This makes it a suitable spin trap for *in vivo* measurements of protein- and DNA-radical adducts. DMPO also diffuses easily through membranes of all cell compartments. Due to its relatively low toxicity, *in vivo* DMPO can be used at concentrations high enough to out-compete the common reactions of DNA radicals, thus ensuring a high yield of DNA nitrone adducts [16-21]. To verify our found result for the DMPO-CHO adduct we used MNP as spin trap for the MNP-CHO adduct with known literature data as well as applied mass spectrometry for the exact mass detection of the reduced DMPO-CHO adduct.

## 2. Material and methods

### *2.1 Chemicals and Reagents*

Solutions were prepared in ultra pure anoxic water from a Millipore Milli-Q ultra-pure water system. All chemicals used were of analytical grade and purchased from Sigma-Aldrich, Germany. MNP was obtained as the dimer, and was used without further purification.

### *2.2 Purification of DMPO*

Prior to experiment, commercially available DMPO was highly purified [22] and the quality checked by EPR. About 1 g charcoal was suspended in 25 ml ice-cold Milli-Q water and flushed with $N_2$ for 10 min. An ampoule DMPO (1 ml) was added to the charcoal suspension and flushed with $N_2$ for 10 min. The whole mix was filtered under $N_2$ flow using Whatman paper filters (45 µm). Aliquots of the filtrate (yield ≈ 18 ml) were frozen at -25°C until use. 100 µl of this solution (c ≈ 345 mM DMPO) was mixed with 1 ml pure HCHO solution (c ≈ 2 M). The anoxic solutions were prepared according to a standard procedure [23, 24].

*2.3 Generation of pure formaldehyde*

Pure formaldehyde (HCHO] was generated from decomposition of ≈ 600 mg paraformaldehyde by heating and flushing the produced HCHO by $N_2$ into 5 ml anoxic water (10 ml bottles, sealed by teflon caps, see Fig. 1).

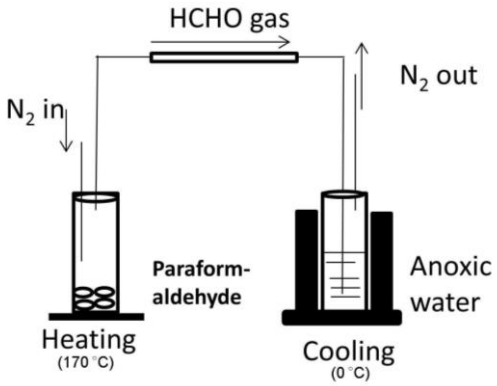


**Fig. 1.** Schematic setup for the generation of pure formaldehyde.

Paraformaldehyd was heated at 170°C under continuous $N_2$ flow, pure formaldehyde was generated and dissolved in anoxic water at 0 °C. The final HCHO concentration obtained was ≈ 2 M and used without further dilution.

*2.4 EPR measurements*

An EPR quartz flat cell (Bruker, ER 160 FC-Q) was filled with mixtures of freshly prepared anoxic 1 ml HCHO (~2 M) solution (Fig. 1) with DMPO or MNP solutions under continuous $N_2$ flow and tightly closed. The formyl radical adducts were produced by UV

radiation. The UV irradiation source was an Osram HNS 10 W/U ofr in a self-made lamp house with a wavelength of 254 nm at an intensity of 35 W/cm$^2$.

About 20 mg MNP-dimer in 6 ml Millipore water were used without further purification for our verification experiment. The solution was treated as described by Makino et. al. [25] 1 ml of this solution (c ≈ 20 mM MNP monomer) was mixed with 1 ml HCHO solution (Fig. 1).

In preliminary experiments we found only weak signals of radicals for the spin trap MNP by photolysis at $\lambda$ = 254 nm. To improve quantum yield from about 30% at 254 nm to ≈ 70% at ≈ 300 nm[26] (see Fig. 2) we later used a XENON 6251 lamp (wavelength range ≈ 200 nm - 2400 nm, Newport Corporation, Darmstadt, Germany; http://www.newport.com).

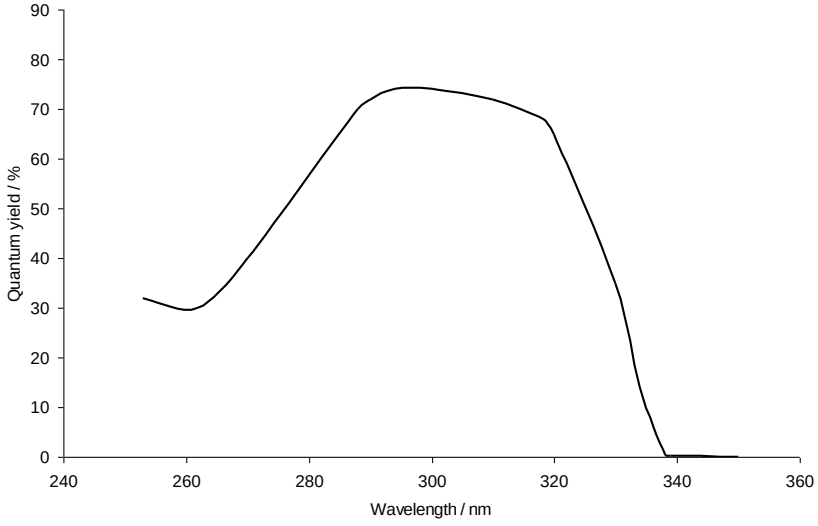


**Fig. 2**. Estimated curve (redrawn) of quantum yield by Calvert et. al. (2011) [26].

175 *2.5 EPR Settings*

176

177 If not otherwise stated, the EPR settings were: microwave power 20 mW, receiver
178 gain $2.5 \cdot 10^4$, center field 3452 G, sweep width 100 G, modulation frequency 100 kHz,
179 modulation amplitude 2 G, conversion time 82 s and time constant 10 s. For noise
180 reduction we accumulated 10 measurements for the DMPO-adducts and 35 for the
181 MNP-adducts. All measurements were carried out on a BRUKER ESP300 instrument in
182 the X-Band regime.

183

184 *2.6 Mass spectrometry measurements*

185

186 To confirm the formation of the described radicals, exact mass measurements and
187 fragmentation experiments of the DMPO-adducts were carried out on a TripleTOF 6600
188 (AB Sciex, Darmstadt, Germany) coupled to a Nexera UPLC (Shimadzu, Duisburg,
189 Germany). Data acquisition and processing were done with Analyst TF 1.7.1.

190

191 **3. Results and Discussion**

192

193 *3.1 EPR spectroscopy after photolysis of formaldehyde by using DMPO*

194

195 UV photolysis of an aqueous solution of pure formaldehyde in presence of DMPO
196 generates the signal shown in Fig. 3. The EPR spectrum was deconvoluted by
197 simulation with the help of EasySpin[27] and WinSim software [28, 29]. We started the
198 simulation of the well-known 1:2:2:1 quartet lines of the DMPO-OH (*) adduct and then

we fitted DMPO-H (▼) [30-32] using literature values. As a result we could identify the 6 lines of the DMPO-CHO (x) adduct with the isotropic hyperfine coupling constants $a_N$ = 15.72 G and $a_H$ = 21.27 G (see Table 1). The best fit resulted in a highly significant root-mean-square R value of 0.997 with a residual value RMSD of 0.097.

The EPR signal is composed of three adduct species, whose spectra overlap (Fig. 4). The relative areas reported by WinSim are: DMPO-CHO ≈ 71%, DMPO-OH ≈ 19%, and for the DMPO-H adduct ≈ 10%. The extracted signals in Fig. 4 were scaled to their relative areas. This makes it easier to show the overlapping of the different species. As seen from Fig. 4 the DMPO-OH adduct (b) overlaps the DMPO-H adduct (c). Due to the continuous generation of $^{\bullet}$CHO, one obtains a strong signal of DMPO-CHO (see also Fig. 3, marked by x symbol).

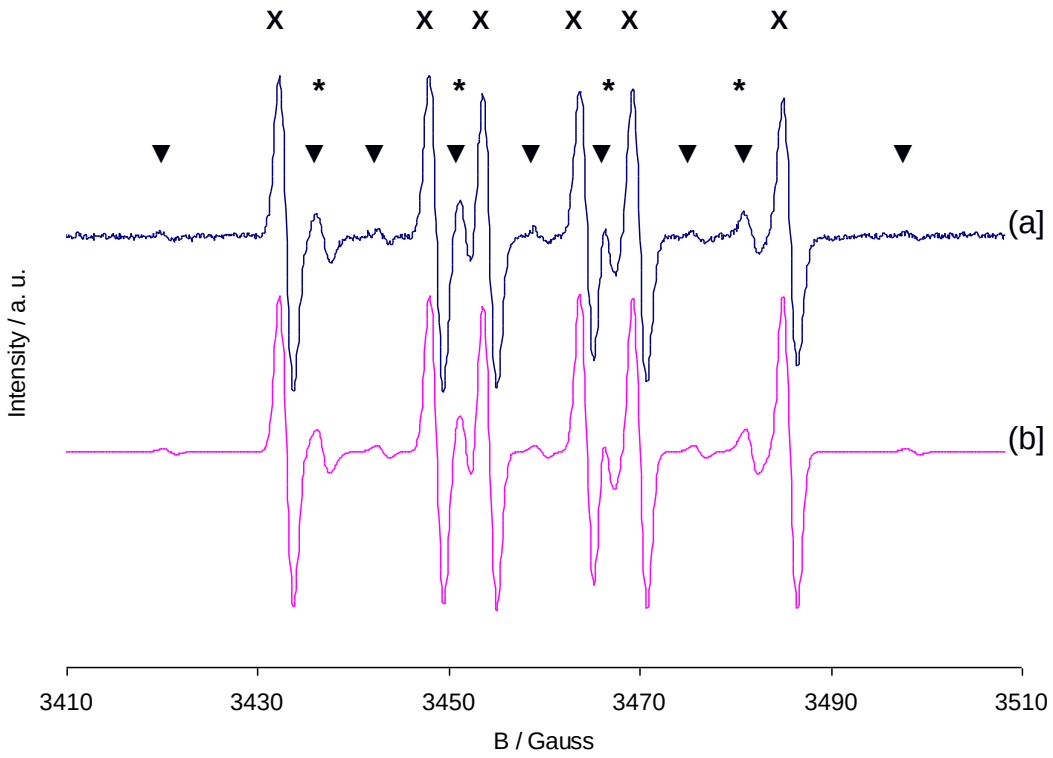


**Fig. 3.** EPR spectrum and simulation obtained by UV photolysis of HCHO. The EPR spectrum in presence of DMPO (a) and the simulation of the measured signal (b) are shown. The spectrum (a) is an accumulation of 10 single measurements. The positions of the adduct signals are marked: (*) DMPO-OH, (▼) DMPO-H and (x) DMPO-CHO. The final concentrations of HCHO and DMPO used were ~1.8 M and ~31 mM, respectively.

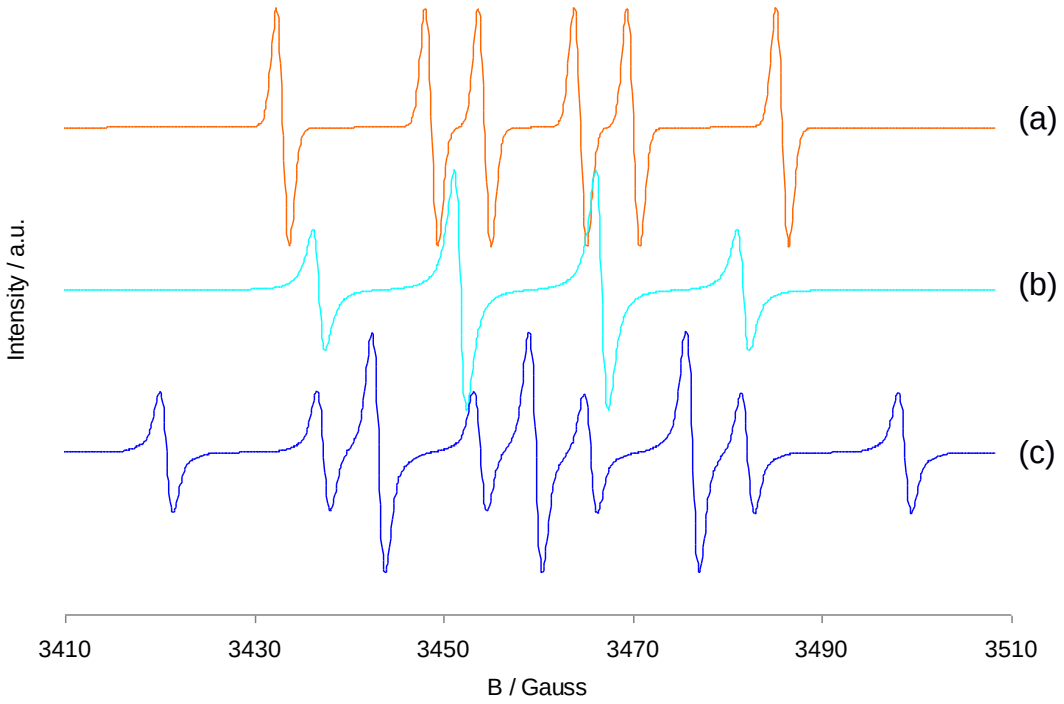


**Fig. 4.** Simulation of deconvoluted spectra of radical adducts using DMPO. The three components of the simulated spectrum (see Fig. 3 (b)) with the DMPO adducts: (a) DMPO-CHO, (b) DMPO-OH and (c) DMPO-H adduct. The maximal values of signals (a) - (c) were scaled to 1.

**Table 1**: Isotropic hyperfine coupling constants and NoH (N over H values) using DMPO. The isotropic hyperfine constants, NoH and literature values for the various DMPO adducts are given.

| Adduct | $a_N$ / Gauss | $a_H$ / Gauss | NoH = $a_N$ / $a_H$ | Ref. |
|---|---|---|---|---|
| DMPO-CHO | 15.72 | 21.27 | 0.74 | this work |
| | 15.80 | 21.10 | 0.75 | 11 |
| DMPO-OH | 14.94 | 14.88 | 1.004 | this work |
| | 14.90 / 15.00 | 14.90 / 15.00 | 1 | 30 / 31 |
| DMPO-H | 16.61 | 22.30 | 0.75 | this work |
| | 16.60 | 22.50 | 0.74 | 30 |
| | 16.60 | 22.60 | 0.73 | 32 |

Lown and Chen [33] assigned their values of $a_N$ = 15.6 G and $a_H$ = 18.8 G erroneously to $^{\bullet}$CHO, but it is obviously the carbon dioxide radical anion ($^{\bullet}CO_2^-$) as deduced from the original publications [34, 35]. We cannot base our simulations on their values for $^{\bullet}$CHO.

A search of the spin trap database [36] with the chemically not-quite correct nomenclature $^{\bullet}$COH yields two results: (1) $a_N$ = 14 G and $a_H$ = 17.7 G [37]. The authors assign their values to the acetyl radical, not to the formyl radical with reference to the following original literature (2) $a_N$ = 14.03 G and $a_H$ = 17.87 G [12]. Here the radicals with these above mentioned values are also annotated to the acetyl radical, requiring correction / update of the spin trap database as search of $^{\bullet}$CHO provides no results with DMPO.

*3.2 EPR spectroscopy after photolysis of formaldehyde by using MNP*

Additionally we verified our results using MNP as spin trap. Literature data are known for the MNP-H and the MNP-CHO adduct (see Table 2) [30, 38, 39]. MNP, a monomer in aqueous solution, itself produces a signal in EPR measurements due to the addition of the carbonaceous dissociation component from MNP [25, 40], assigned as MNP-2-methyl-2-propyl (MNP-MP] adduct (see below]. The chemistry of MNP is shown in Scheme 2.

**Scheme 2**. Chemistry of the MNP spin trap. (1) Equilibrium reaction of MNP dimer and MNP monomer in aqueous solution. (2) reaction of MNP monomer with UV light to 2-methyl-2-propyl (MP) radical and nitric oxide radical and (3) reaction of MNP with 2-methyl-2-propyl radical to the MNP-MP adduct.

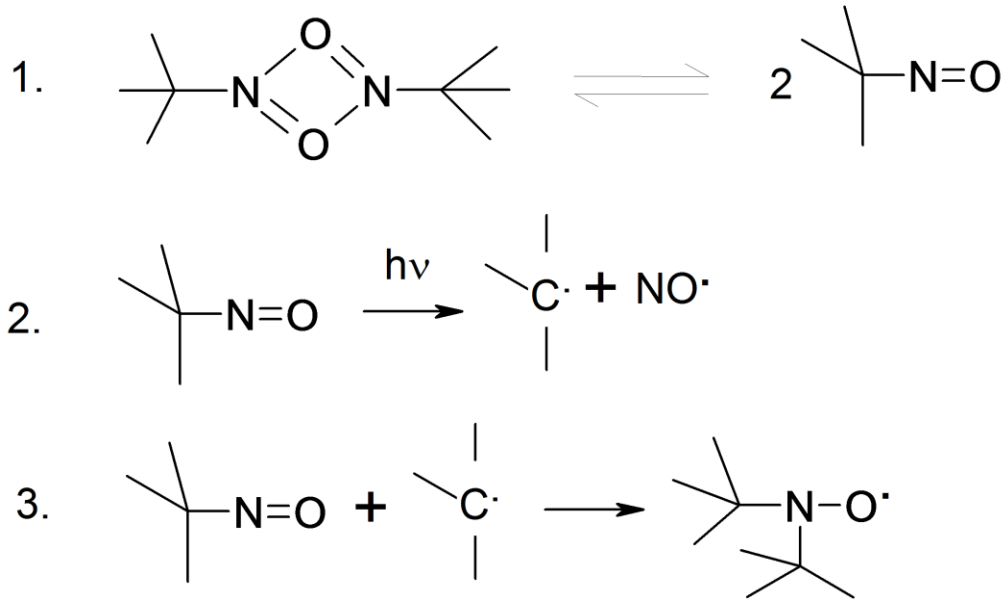

In preliminary experiments, we have obtained very small signal intensities at 254 nm for MNP. A literature search has shown that the quantum yield for the reaction

$$HCHO \xrightarrow{h\nu} {}^{\bullet}CHO + {}^{\bullet}H$$

increased from about 30% at 254 nm to approximately 70% at 300 nm UV radiation [26] (Fig. 2]. The measured EPR spectrum (a] and the simulation (R = 0.97] of the signal (b] are presented in Fig. 5. The arrows indicate the position of the MNP-CHO adduct overlapped by MNP-MP and MNP-H. EPR signals are additive. Therefore the MNP-CHO signal is disturbed by the overlapping of the MNP-MP and MNP-H signals.

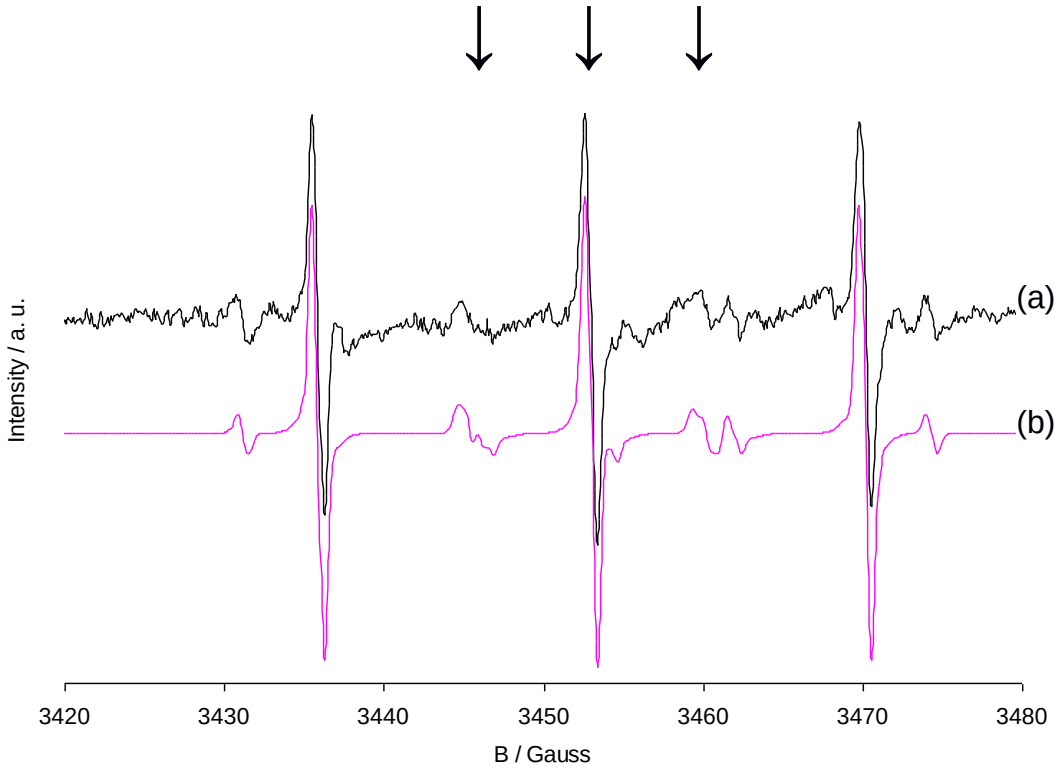


**Fig. 5.** EPR spectrum and simulation obtained by UV photolysis of HCHO using MNP. EPR spectrum in presence of MNP (a) and the simulation of the signals (b) are exhibited. The arrows indicate the position of the MNP-CHO adduct (35 accumulations) overlapped by MNP-MP and MNP-H. The final concentrations of HCHO and MNP-monomer used were ~1 M and ~10 mM, respectively.

Again, we deconvoluted the MNP's EPR spectrum, using the simulation tools EasySpin and WinSim software [27-29]. The signal was identified to consist of three components: the MNP-MP, MNP-CHO and MNP-H adducts (Fig. 6). Simulations using WinSim yielded relative areas of MNP-MP ≈ 73%, MNP-CHO ≈ 18% and MNP-H ≈ 9%. The simulated signals in Fig. 6 were again scaled to their relative areas. As it can be seen from Fig. 5 and 6, the MNP-CHO adduct is strongly overlapped by MNP-MP and MNP-H.

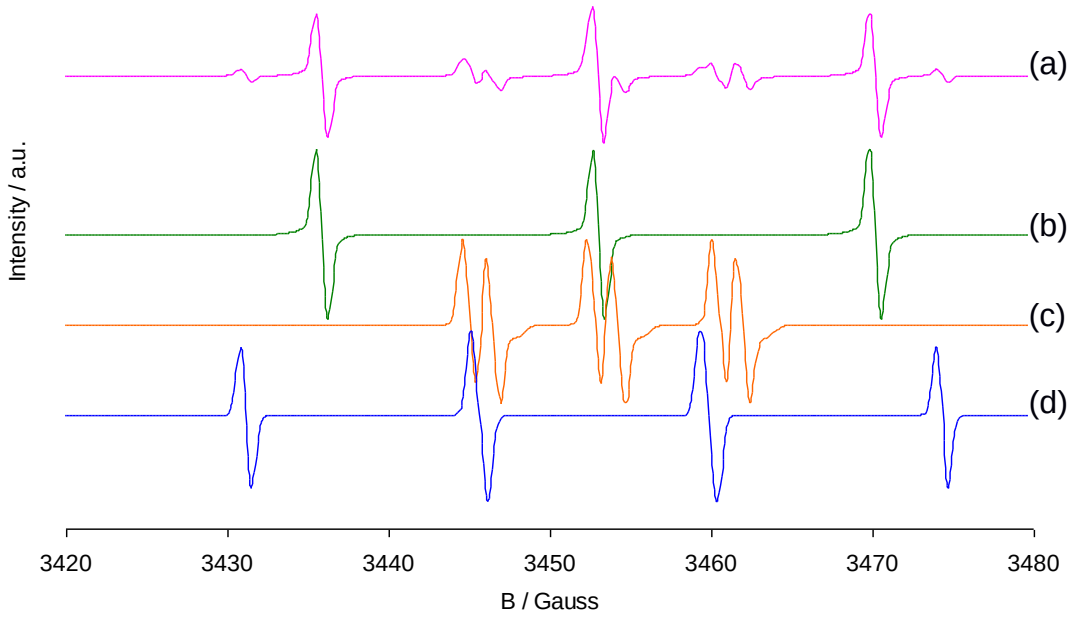


**Fig. 6**. Simulated spectrum and deconvoluted signals of all adducts with MNP. (a) The simulated spectrum of all components (no scaling, see also Fig. 5(b)) and the three components of the MNP adducts: (b) MNP-MP, (c) MNP-CHO and (d) MNP-H are shown. The maximal values of signals (b) - (d) were scaled to 1.

**Table 2**: Isotropic hyperfine coupling constants and NoH values using MNP. The isotropic hyperfine coupling constants, NoH and literature values of MNP-MP and other MNP adducts are given.

| Adduct | $a_N$ / Gauss | $a_H$ / Gauss | NoH | Ref. |
|---|---|---|---|---|
| MNP-MP | 17.14 | - | - | this work |
| | 17.20 | - | - | 40 |
| MNP-CHO | 7.74 | 1.44 | 5.38 | this work |
| | 6.90 - 7.70 | 1.40 - 2.50 | 2.92 - 5.29 | 30 / 38 / 39 |
| MNP-H | 14.20 | 14.72 | 0.97 | this work |
| | 14.40 | 14.40 | 1.00 | 30 |

In the following section we describe the result of our mass spectrometry experiment. Fig. 7 illustrates the MS/MS mass spectrum with the exact mass of the reduced DMPO-CHO adduct.

*3.2 Mass spectrometry*

The characteristic fragments of the DMPO moiety and the loss of -OH and -CHO in the final product of “DMPO-CHO” (Fig. 7] as compared to the “DMPO-OH” and DMPO mass spectra found, confirm the results of EPR measurements and simulations.

The mass fragments and the typical relative intensities of the reduced final product “DMPO-CHO” are:

ESI-MS (positive mode]: HRMS *m/z* 144.1011 (calculated mass for $[C_7H_{14}NO_2]^+$ *m/z* 144.1019]; MS/MS (CE 20V; $[M+H]^+$ *m/z* (%]:126.092 (100], 81.069 (69], 144.102 (67], 93.068 (49], 79.054 (47], 98.096 (43], 109.063 (37], 108.078 (31], 77.038 (28], 91.053 (26], 82.064 (25], 69.070 (22], 84.081 (22], 53.038 (22], 56.0498 (21].

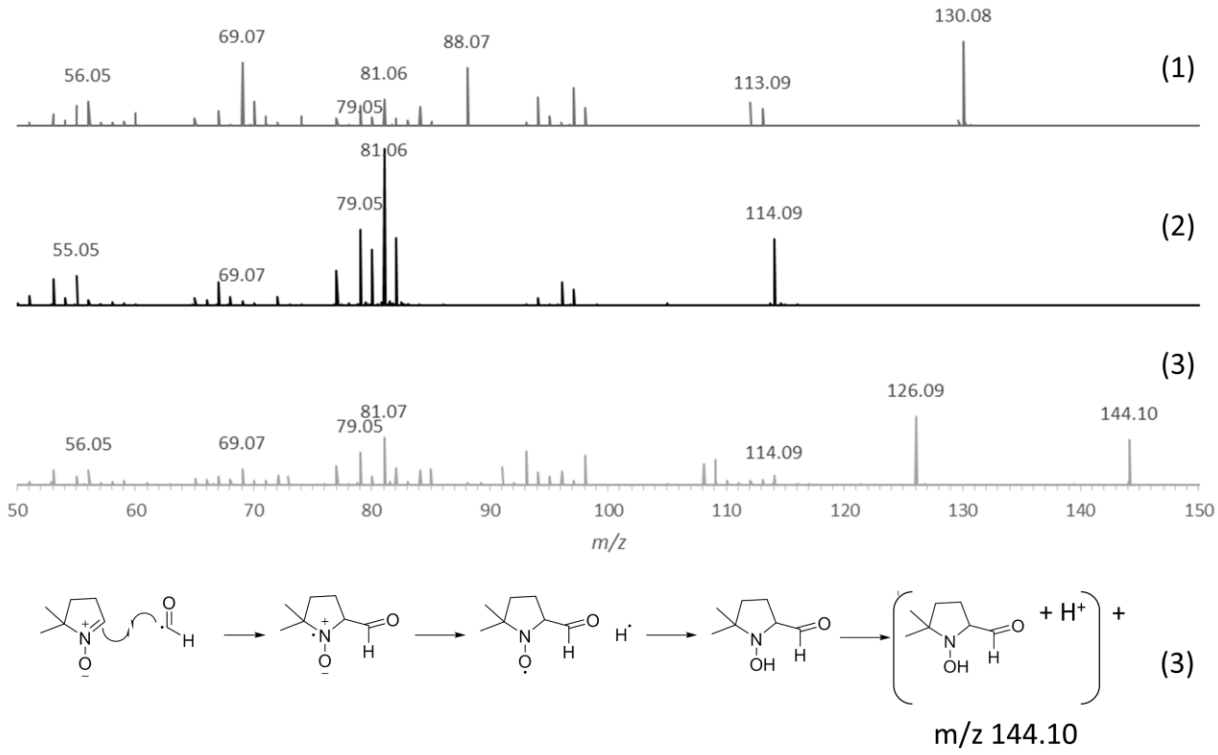


**Fig. 7**. MS/MS mass spectra and reaction mechanism sequence proving the formation of DMPO-CHO adduct. The exact mass of the reduced DMPO-CHO adduct (3] is given as compared to DMPO-OH adduct (1) and DMPO (2) after protonation. The final product (reduced DMPO-CHO adduct) was formed by the attack of •CHO and •H and later protonated to give the mass m/z 144.10 as shown in the reaction mechanism below (3).

The reaction mechanisms of formation of DMPO-OH adduct were already described by Yang et al. [41].

### *3.4 Significance and potential of detection of DMPO-formyl radical adduct*

We showed unambiguously in the first step that the formyl radical could be generated from formaldehyde at ambient temperature under photolytic conditions similar to that of UV-B band radiation of sun light (Fig. 2). As the life span of formyl radical is extremely short [8], we must rather have more sensitive techniques to show the *in vivo* formation of DMPO-formyl radical adduct (Fig. 7), e. g. mass spectrometry after oxidation into more stable Nitrone adduct and/or probably by immunological techniques [42, 43]. Our results point to formyl radical formation from formaldehyde under ambient conditions that could be related to the carcinogenesis of formaldehyde, already associated with e.g. different types of cancer, diabetes, Alzheimer disease [44 - 47].

## 4. Conclusions

To summarize, we can conclude that we have provided the unambiguous experimental identification and the signal simulation of DMPO-CHO adduct in order to detect the formyl radical $^{\bullet}$CHO with the spin trap DMPO at ambient temperature in anoxic aqueous solution without using any catalysator(s). Since the formyl radical gives a signal with low intensity at ambient temperature that is almost overlapped by DMPO-H and DMPO-OH, an experimental approach was needed that continuously generates radicals in a closed system and minimizes noise. Independent mass spectrometry using

406 TripleTOF-MS validated the results of formyl radical formation as shown by EPR
407 experiments and simulation data, too. Based on our results, the detection of •CHO with
408 DMPO can be recommended because it is relatively non-toxic [19] and it produces also
409 stable adducts. The isotropic hyperfine constants derived from our EPR study for
410 DMPO-adducts can now be used for the *in vitro* characterization of formyl radical at
411 ambient temperature. Our studies also show the possibility of using DMPO as an
412 endogenous trap of formyl radical for future use *in vivo* studies in connection with
413 various severe diseases like cancer, diabetes, Alzheimer disease [44 - 47]. For this
414 purpose, formyl-DMPO radical adduct can be measured either by TripleTOF-MS (see
415 above), or probably by immuno-fluorescence analysis of fluorescence-labelled antibody
416 for specific detection of bound anti-DMPO probe in tissues [42, 43].
417
418 **Notes**
419 The authors declare no competing financial interest.
420
421 **Acknowledgements**
422 We thank Wolf Bors, Christa Michel and Werner Heller for helpful discussion and
423 Albrecht Wieser for his permission and cooperation to use his EPR machine**.** We are
424 grateful to Garry Buettner for his critical reading and valuable comments. The authors
425 wish to thank SCIEX Darmstadt, Germany, for providing technical and application
426 support.
427
428

## References


[1] Haber, L. C.; Vandsburger, U. A global reaction model for oh* chemiluminescene applied to a laminar flat-flame burner. *Combust. Sci. Technol.* **2003**, *175*, 1859 - 1891.

[2] Bartels, M.; Edelbüttel-Einhaus, J.; Hoyermann, K. The detection of $CH_3CO$, $C_2H_5$, and $CH_3CHO$ by rempi/mass spectrometry and the application to the study of the reactions $H+CH_3CO$ and $O+CH_3CO$. *Symp. Int. Combust.* **1991**, *23*, 131 - 138.

[3] Burcat, A.; Radhakrishnan, K. High temperature oxidation of propene. *Combust. Flame* **1985**, *60*, 157 - 169.

[4] Marcker, K.; Sanger, F. N-formyl-methionyl-S-RNA. *J. Mol. Biol.* **1964**, *8*, 835 - 840.

[5] Wolan, D. W.; Greasley, S. E.; Beardsley, G. P.; Wilson, I. A. Structural insights into the Avian AICAR transformylase mechanism. *Biochemistry* **2002**, *41*, 15505 - 15513.

[6] Holmberg, R. W. ESR study of $H\dot{C}O$ in single crystals of formic acid at 77°K. *J. Chem. Phys*. **1969**, *51*, 3255 - 3260.

[7] Gomes, J. R. B.; Gomes, J. A. N. F. Adsorption of the formyl species on transition metal surfaces. *J. Electroanal. Chem.* **2000**, *483*, 180 - 187.

[8] Adrian, F. J.; Cochran, E. L.; Bowers, V. A. ESR spectrum and structure of the formyl radical. *J. Chem. Phys.* **1962**, *36*, 1661 - 1672.

[9] Snyder, L. E.; Hollis, J. M.; Ulich, B. L. Radio detection of the interstellar formyl radical. *Astrophys. J.* **1976**, *208*, L91 - L94.

[10] *Cancer Biology, a Study of Cancer Pathogenesis. How to prevent Cancer and Diseases*; Migdalia, A., Ed.; Xlibris Corp.: USA, 2011.

[11] Yang, J.; Dongxu, L.; Zhang, Z.; Li, Q.; Wang, H. A study of the photocatalytic oxidation of formaldehyde on $Pt/Fe_2O_3/TiO_2$. *Photochem. Photobiol. A: Chemistry* **2000**, *137*, 197 - 202.

[12] Janzen, E. G.; Liu, J. I-P. Radical addition reactions of 5,5-dimethyl-1-pyrroline-1-oxide. Spin trapping with a cyclic nitrone. *J. Magn. Reson*. **1973**, *9*, 510 - 512.

[13] Janzen, E. G.; Stronks, H. J.; Dubose, C. M.; Poyer, J. L.; McCayt, P. B. Chemistry and biology of spin-trapping radicals associated with halocarbon metabolism *in vitro* and *in vivo*. *Environmental Health Perspectives* **1985**, *64*, 151 - 170.

[14] Levine, J. S. In *The Photochemistry of Atmospheres*; Levine, J. S., Ed.; Academic Press Inc.: London, Ltd., 1985; pp 3 - 38.

[15] Weber, G. F. The measurement of oxygen-derived free radicals and related substances in medicine. *J. Clin. Chem. Clin. Biochem.* **1990**, *28*, 569 - 603.

[16] Morgan, D. D.; Mendenhall, C. L.; Bobst, A. M.; Rouster, S. D. Incorporation of the spin trap DMPO into cultured fetal mouse liver cells. *Photochem. Photobiol.* **1985**, *42*, 93 - 94.

[17] Sanmartín-Suárez, C.; Soto-Otero, R.; Sánchez-Sellero, I.; Méndez-Álvarez, E. Antioxidant properties of dimethyl sulfoxide and its viability as a solvent in the evaluation of neuroprotective antioxidants. *J. Pharmacol. Toxicol. Methods* **2011**, *63*, 209 - 215.

[18] Hawkins, C. L.; Davies, M. J. Generation and propagation of radical reactions on proteins. *Biochim. Biophys. Acta* **2001**, *1504*, 196 - 219.

[19] Janzen, E. G.; Poyer, J. L.; Schaefer, C. F.; Downs, P. E.; DuBose, C. M. Biological spin trapping II. Toxicity of nitrone spin traps: Dose-ranging in the rat. *J. Biochem. Biophys. Methods*. **1995**, *30*, 239 - 247.

[20] Davies, M. J.; Hawkins, C. L. EPR spin trapping of protein radicals. *Free Radical Biol. Med.* **2004**, *36*, 1072 - 1086.

[21] Ramirez, D. C.; Gomez-Mejiba, S. E; Mason, R. P. Immuno-spin trapping analyses of DNA radicals. *Nat. Protoc.* **2007**, *2*, 512 - 522.

[22] Buettner, G. R.; Oberley, L. W. Considerations in the spin trapping of superoxide and hydroxyl radical in aqueous systems using 5,5-dimethyl-1-pyrroline-1-oxide. *Biochem. Biophys. Res. Commun.* **1978**, *83*, 69 - 74.

[23] Hungate, R. E. In *Methods in Microbiology*; Norris, J. R.; Ribbons, D. W. Eds.; Academic Press Inc.: London, Ltd., 1969; Vol. 3, part B, pp 117 - 132.

[24] Widdel, F. Anaerober Abbau von Fettsäuren und Benzoesäure durch neu isolierte Arten Sulfat-reduzierender Bakterien. Ph.D. Dissertation, Georg-August-Universität Göttingen, Germany, **1980**.

[25] Makino, K.; Suzuki, N.; Moriya, F.; Rokushika, S.; Hatano, H. A fundamental study on aqueous solutions of 2-methyl-2-nitrosopropane as a spin trap. *Radiat. Res.* **1981**, *86*, 294 - 310.

[26] *The Mechanisms of Atmospheric Oxidation of the Oxygenates*; Calvert, J. G., Mellouki, A., Orlando, J. J., Eds. Oxford University Press Inc.: New York, 2011; p. 986.

[27] Stoll, S.; Schweiger, A. EasySpin, a comprehensive software package for spectral simulation and analysis in EPR. *J. Magn. Reson.* **2006**, *178*, 42 - 55.

[28] O'Brien, D. A.; Duling, D. R; Fann, Y. C. NIEHS, USA. http://www.niehs.nih.gov/research/resources/software/tox-pharm/tools/index.cfm (accessed October 2015).

[29] Duling, D. R. Simulation of multiple isotropic spin trap EPR spectra. *J. Mag. Reson. Ser B* **1994**, *104*, 105 - 110.

[30] Buettner, G. R. Spin trapping: ESR parameters of spin adducts. *Free Radical Biol. Med.* **1987**, *3*, 259 - 303.

[31] Makino, K.; Mossaba, M. M.; Riez, P. Chemical effects of ultrasound on aqueous solutions. Evidence for $^{\cdot}OH$ and $^{\cdot}H$ by spin trapping. *J. Am. Chem. Soc*. **1982**, *104*, 3536 - 3539.

[32] Yoo, D. H.; Han, S. K.; Lee, M. J.; Kang, J. W. Spin trapping EPR method for simultaneous monitoring of hydroxyl radicals and hydrogen atoms in γ-irradiation process. *J. Ind. Eng. Chem.* **2005**, *11*, 215 - 221.

[33] Lown, J. W.; Chen, H. Evidence for the generation of free hydroxyl radicals from certain quinine antitumor antibiotics upon reductive activation in solution. *Can. J. Chem.* **1981**, *59*, 390 - 395.

[34] Harbour, J. R.; Hair, M. L. Spin trapping of the $^{\bullet}CO_2^-$ radical in aqueous solution. *Can. J. Chem.* **1979**, *57*, 1150 - 1152.

[35] Harbour, J. R.; Chow, V.; Bolton, J. R. An Electron Spin Resonance study of the spin adducts of OH and $HO_2$ radicals with nitrones in the ultraviolet photolysis of aqueous hydrogen peroxide solutions. *Can. J. Chem.* **1974**, *52*, 3549 - 3553.

[36] Spin Trap Database, NIEHS, USA. http://tools.niehs.nih.gov/stdb/index.cfm (accessed January 2017].

[37] Pryor, W. A.; Govindan, C. K.; Church, D. F. Mechanism of ozonolysis of acetylenes; evidence for a free-radical pathway for the decomposition of intermediates. *J. Am. Chem. Soc.* **1982**, *104*, 7563 - 7566.

[38] Janzen, E. G.; Lopp, I. G.; Morgan, T. V. Detection of fluoroalkyl and acyl radicals in the gas-phase photolysis of ketones and aldehydes by Electron Spin Resonance gas-phase spin trapping techniques. *J. Phys. Chem*. **1973**, *77*, 139 - 141.

[39] Heinzel, A.; Holze, R.; Hamann, C. H.; Blum, J. K. The electrooxidation of methanol and formaldehyde at a platinium electrode: A SEERS study of radical intermediates - I. *Electrochim. Acta* **1989**, *34*, 657 - 661.

[40] Massari, J.; Tokikawa, R.; Medinas, D. B.; Angeli, J. P. F; Mascio, P. D.; Assunção, N. A.; Bechara, E. J. H. Generation of singlet oxygen by the glyoxal-peroxynitrite system. *J. Am. Chem. Soc.* **2011**, *133*, 20761 - 20768.

[41] Yang, F.; Zhang, R.; He, J.; Abliz, Z. Development of a liquid chromatography/electrospray ionization tandem mass spectrometric method for the determination of hydroxyl radical. *Rapid Commun. Mass Spectrom.* **2007**, *21*, 107 - 111.

[42] Towner, R. A.; Smith, N.; Saunders, D.; Henderson, M.; Downum, K.; Lupu, F.; Silasi-Mansat, R.; Ramirez, D.C.; Gomez-Mejiba, S. E.; Bonini, M. G.; Ehrenshaft, M.; Mason, R.P. In vivo imaging of immuno-spin trapped radicals with molecular magnetic resonance imaging in a diabetic mouse model. *Diabetes* **2012**, *61*, 2405 - 2413.

[43] Mason, R. P. Imaging free radicals in organelles, cells, tissue, and in vivo with immuno-spin trapping. *Redox Biology* **2016**, *8*, 422 - 429.

[44] Kato, S.; Burke, P. J.; Koch, T. H.; Bierbaum, V. M. Formaldehyde in Human Cancer Cells: Detection by Preconcentration-Chemical Ionization Mass Spectrometry. *Anal. Chem.* **2001**, *73*, 2992 - 2997.

548 [45] Tong, Z.; Luo, W.; Wang, Y.; Yang, F.; Han, Y.; Li, H.; Luo, H.; Duan, B.; Xu, T.;
549 Maoying, Q.; Tan, H.; Wang, J.; Zhao, H.; Liu, F.; Wan, Y. Tumor Tissue-Derived
550 Formaldehyde and Acidic Microenvironment Synergistically Induce Bone Cancer
551 Pain. *PLoS ONE* **2010**, *5*, 1 - 15.
552 [46] Lee, Y. H.; Tang, Y.; Verwilst, P.; Lin, W.; Kim, J. S. A biotin-guided formaldehyde
553 sensor selectively detecting endogenous concentrations in cancerous cells and
554 tissues. *Chem. Commun*. **2016**, *52*, 11247 - 11250.
555 [47] Tong, Z. Urine Formaldehyde: A Non-Invasive Marker for Alzheimer's Disease?
556 *J Alzheimers Dis Parkinsonism* **2017**, 7, 1000345.